

# Trifocal Tensor for Heterogeneous Cameras

SriRam Thirthala  
tvn@cs.unc.edu

Marc Pollefeys  
marc@cs.unc.edu

## Abstract

*We study the multi-view geometry arising out of a setup consisting of a pin-hole camera and two 1D radial cameras. A broad class of both central and non-central cameras, such as fish-eye and catadioptric cameras, can be reduced to 1D radial cameras under the assumption of known center of radial distortion. For cameras in general configuration, we introduce the mixed trifocal tensor which can be computed from 10 or more features seen in these three heterogeneous views. We show that the mixed trifocal tensor has only one internal constraint (in contrast to the standard trifocal tensor that has 8). We characterise this internal constraint and show that enforcing it can be reduced to solving the standard Quadratic Eigenvalue Problem (QEP). We analyse the (practically useful) special case when the optical axes of the two radial cameras intersect at a point. We show that enforcing this constraint can be reduced to solving the standard Two-Parameter Eigenvalue Problem. Further, we demonstrate that the Fundamental Matrix is embedded in the mixed trifocal tensor in this special case. In this paper, we are mainly concerned with the theoretical aspects of the mixed trifocal tensor and thus no experimental results are reported.*

## 1. Introduction

There has been a growing interest in the vision community for omnidirectional cameras. By providing a wider field of view these cameras are more suited for a range of applications. Two different approaches are used to obtain a wider field of view. The first approach consists of using a fish-eye lens which typically yields a field of view of around 180 degrees. The second approach consists of using a camera in combination with a curved mirror to obtain a catadioptric camera. The mirror surface is typically a quadric that is symmetric around the optical axis of the camera. Based on the position of the camera center, one obtains a central [1] or non-central camera [18, 10]. A broad class of omnidirectional cameras can be reduced to 1D radial cameras (discussed in Section 2) under the assumption of known center of radial distortion.

The advantage of wider field of view has encouraged the use of omnidirectional cameras in camera networks.

Further, many camera networks these days are hybrid and consist of a combination of pin-hole and omnidirectional cameras. The main topic of this paper is the analysis of the multi-view constraints arising out of a setup consisting of one pin-hole camera and two omnidirectional cameras (modeled as 1D radial cameras).

Many different techniques have been proposed to calibrate omnidirectional cameras. Some require knowledge about the scene or camera motion [16, 19, 4, 2, 13, 6, 25, 12, 24] while others do so based only on feature correspondences [5, 14]. Besides these, there has also been work on generalized camera models. All the approaches that have been proposed for this require knowledge about the scene structure or camera motion [7, 17]. There has been a lot of work on calibrating camera networks. However very few have addressed the calibration of hybrid networks. Chen et al. [3] have recently proposed a technique to calibrate a network consisting of a single catadioptric camera and many pin-hole cameras. They first calibrate the catadioptric camera individually. Then using known scene information they are able to calibrate the other perspective cameras. The approach that we propose here uses only feature correspondences among the pin-hole camera and the two omnidirectional cameras. Further, we use the radial 1D camera model which is sufficiently general to model most omnidirectional cameras. The main application of our work would be in large hybrid camera networks where there would be patches of the scene which are visible from two omnidirectional cameras and a pin-hole camera.

## 2. Radial 1D Camera

Suppose that the center of radial distortion is known. For most omnidirectional cameras the image center is a good approximation for the center of distortion [23].<sup>1</sup> The image can then be transformed such that the center of radial distortion is the origin.

Consider a point in the world  $\mathbf{X}$  that projects onto  $\mathbf{x}_d = (x_d, y_d, 1)^T$  in the distorted (input) image. Further let  $\mathbf{C}$  be the camera center. Because of large unknown and possibly varying distortion, the point  $\mathbf{X}$  does not lie on the ray

---

<sup>1</sup>However if additional information is known, for example if one can see the rim of a fish-eye lens or the rim of a curved mirror, the center of the rim can be used as a better approximation for the center of radial distortion.

passing through  $C$  and  $\mathbf{x}_d$  (see Figure 1(a)).

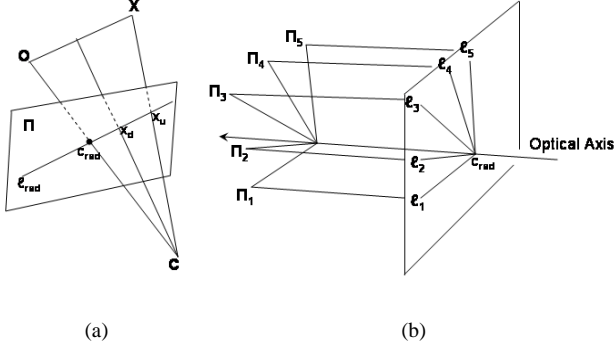


Figure 1: *Radial 1D Camera*

However, consider the line passing through the center of radial distortion and  $\mathbf{x}_d$  in the image ( $\mathbf{l}_{rad} = \mathbf{x}_d \times \mathbf{c}_{rad}$ ). The undistorted image point (one that would have been obtained if the camera had followed a pin-hole projection model)  $\mathbf{x}_u$ , would lie on this line. This is because though the *distance* of an image point from the center of radial distortion is not preserved by radial distortion, the *direction* (which is what the radial line  $\mathbf{l}_{rad}$  encodes) is. If instead of back-projecting a ray, we back-project the line  $\mathbf{l}_{rad}$  using the camera center, it would contain the ray passing through  $C$  and  $\mathbf{x}_u$ , and thus would contain  $\mathbf{X}$ .

Thus, by representing the distorted image as a 1D image of radial lines passing through the center of radial distortion, we can factor out the *unknown deviation* from the pin-hole model (which is along the radial line), but preserve the *known information* (direction of radial line). The radial 1D camera can be thought of as projecting the bundle of planes containing the optical axis onto the bundle of lines passing through the  $\mathbf{c}_{rad}$  (Figure 1(b)). A radial line can be represented as  $\mathbf{l} = (y, -x)^T$  if  $\mathbf{c}_{rad}$  has been mapped to the origin. Note that a radial 1D camera can be obtained for almost all single effective viewpoint cameras (standard pin-hole cameras, low radial distortion cameras, fish-eye lenses, catadioptric cameras [1]). Infact, we can also deal with non-central cameras. The only requirement is that all points that lie in one plane of the bundle around the optical axis, project onto the same radial line (passing through  $\mathbf{c}_{rad}$ ). For catadioptric systems, this corresponds to the requirement that all the normals on the mirror have to be contained within radial planes. This constraint is automatically satisfied for mirror shapes that are symmetric around the optical axis.

**Definition:** The radial 1D camera represents the mapping of a point in  $P^3$  onto a radial line in the image. Since it is a  $P^3 \rightarrow P^1$ , it can be represented by a  $2 \times 4$  matrix and has 7 degrees of freedom.

The projection of a 3D point  $\mathbf{X}$  on a radial line  $\mathbf{l}$  using

radial camera  $\mathbf{P}$  is then given by:

$$\lambda \mathbf{l} = \mathbf{P} \mathbf{X} \quad (1)$$

with  $\lambda$  a non-zero scale factor. Note that a point  $\mathbf{O}$  on the optical axis does not have a proper image in  $P^1$  as we obtain  $\mathbf{P} \mathbf{O} = (0, 0)^T$ .

### 3. Mixed Trifocal Tensor

Consider the point  $\mathbf{X}$  that projects onto the point  $\mathbf{x}_{3 \times 1}$  in the pin-hole camera and the radial lines  $\mathbf{l}'_{2 \times 1}$  and  $\mathbf{l}''$  in the radial cameras. Then it projects by the following set of equations,

$$\begin{aligned} \lambda \mathbf{x} &= \mathbf{P}_{3 \times 4} \mathbf{X} \\ \lambda' \mathbf{l}' &= \mathbf{P}'_{2 \times 4} \mathbf{X} \\ \lambda'' \mathbf{l}'' &= \mathbf{P}''_{2 \times 4} \mathbf{X} \end{aligned} \quad (2)$$

These equations can be rewritten in matrix format as,

$$\begin{bmatrix} \mathbf{P}_{3 \times 4} & \mathbf{x} & \mathbf{0} & \mathbf{0} \\ \mathbf{P}'_{2 \times 4} & \mathbf{0} & \mathbf{l}' & \mathbf{0} \\ \mathbf{P}''_{2 \times 4} & \mathbf{0} & \mathbf{0} & \mathbf{l}'' \end{bmatrix} \begin{bmatrix} \mathbf{X} \\ -\lambda \\ -\lambda' \\ -\lambda'' \end{bmatrix} = \mathbf{0} \quad (3)$$

Since we know that a solution exists, the right null-space of the  $7 \times 7$  measurement matrix should have non-zero dimension, which implies that

$$\det \begin{bmatrix} \mathbf{P}_{3 \times 4} & \mathbf{x} & \mathbf{0} & \mathbf{0} \\ \mathbf{P}'_{2 \times 4} & \mathbf{0} & \mathbf{l}' & \mathbf{0} \\ \mathbf{P}''_{2 \times 4} & \mathbf{0} & \mathbf{0} & \mathbf{l}'' \end{bmatrix} = 0 \quad (4)$$

Following the approach of [21], expansion of the determinant produces the unique trilinear constraint for the pin-hole view and the two 1D views,

$$\mathbf{T}_i^{jk} \mathbf{x}^i \mathbf{l}'_j \mathbf{l}''_k = 0 \quad (5)$$

We use the Einstein summation convention in which indices repeated in covariant and contravariant positions denote implicit summations.

$\mathbf{T}_i^{jk}$  is the  $3 \times 2 \times 2$  mixed trifocal tensor for the pin-hole camera and two 1D radial cameras. Elements of  $\mathbf{T}$  can be written as  $4 \times 4$  minors of the joint projection matrix  $\left[ \mathbf{P}^T \mathbf{P}'^T \mathbf{P}''^T \right]^T$  where two rows (of the minor) come from the pin-hole projection matrix,  $\mathbf{P}$ , and a row each is contributed by  $\mathbf{P}'$  and  $\mathbf{P}''$ .

One useful way of understanding the mixed trifocal tensor is by considering the intersection of the ray back-projected from the pin-hole camera and the planes back-projected from the two radial cameras, in 3D space. The back-projected ray intersects the plane back-projected from the first radial camera at a point, say  $\mathbf{X}$ . This constrains the radial line in the second radial camera to be such that the

plane back-projected from it contains  $\mathbf{X}$ . The mixed trifocal tensor captures this incidence relationship.

The mixed trifocal tensor has  $3 \times 2 \times 2 - 1 = 11$  degrees of freedom. Subtracting from these the degrees of freedom required to describe one pin-hole camera and two radial cameras upto a 3D projectivity,  $(3 \times 4 - 1) + 2 \times (2 \times 4 - 1) - (4 \times 4 - 1) = 10$ , we observe that the mixed trifocal tensor has *only one* internal constraint.

### 3.1. Nature of the Internal Constraint

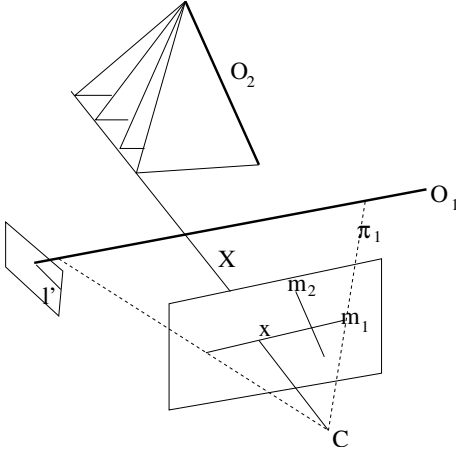


Figure 2:  $\mathbf{O}_1$  and  $\mathbf{O}_2$  are the two optical axes.  $\mathbf{C}$  is the center of the pin-hole camera.  $\Pi_1$  is the plane defined by  $\mathbf{C}$  and  $\mathbf{O}_1$ . Planes  $\Pi_i$  project onto  $\mathbf{m}_i$  in the pin-hole image.  $\mathbf{X}$  (lying on  $\Pi_1$ ) projects onto  $\mathbf{x}$  in the pin-hole image and  $l'$  in the first radial image. The intersection of  $\Pi_1$  (the plane back-projected from  $l'$ ) and the ray back-projected from  $\mathbf{x}$  is the ray itself. Any plane back-projected from the second radial camera will intersect this ray.

We will now characterise the internal constraint of the mixed trifocal tensor. Consider Figure 2. Let  $\mathbf{C}$  be the camera center of the pin-hole camera and  $\mathbf{O}_1$  and  $\mathbf{O}_2$  be the optical axes of the two radial cameras. Let us denote the plane defined by  $\mathbf{C}$  and  $\mathbf{O}_i$  by  $\Pi_i$ .

Consider a point  $\mathbf{X}$ , lying in  $\Pi_1$ , that projects onto  $\mathbf{x}$  in the pin-hole image and  $l'$  in the first radial image. Note that the plane back-projected from the first radial image is  $\Pi_1$ . Further, the ray back-projected from the pin-hole image lies in  $\Pi_1$ . Thus the intersection of these two is the ray itself. Since in 3D space a ray and a plane always intersect, we can choose any arbitrary plane from the bundle back-projected by the second radial camera. This is equivalent to selecting an arbitrary  $l'' = [l''_1, l''_2]$ . This implies that their coefficients in Eq. (5) are zero.

$$\mathbf{T}_i^{j1} \mathbf{x}^i l'_j = 0 \quad \mathbf{T}_i^{j2} \mathbf{x}^i l'_j = 0 \quad (6)$$

Eq. (6) can be interpreted to imply that *there exists*  $l' = [l'_1, l'_2]$  such that

$$\underbrace{\begin{bmatrix} \mathbf{T}_i^{11} \mathbf{x}^i & \mathbf{T}_i^{21} \mathbf{x}^i \\ \mathbf{T}_i^{12} \mathbf{x}^i & \mathbf{T}_i^{22} \mathbf{x}^i \end{bmatrix}}_{\mathbf{M}} \begin{bmatrix} l'_1 \\ l'_2 \end{bmatrix} = \begin{bmatrix} 0 \\ 0 \end{bmatrix} \quad (7)$$

Since the right null-space of the  $\mathbf{M}$  is of non-zero dimension, it implies that  $\det(\mathbf{M}) = 0$ . Thus,

$$\mathbf{T}_p^{11} \mathbf{x}^p \mathbf{T}_q^{22} \mathbf{x}^q - \mathbf{T}_p^{12} \mathbf{x}^p \mathbf{T}_q^{21} \mathbf{x}^q = 0 \quad (8)$$

Note that the above equation is a conic in  $\mathbf{x}$  of the form  $\mathbf{x}^T \mathbf{W} \mathbf{x} = 0$  where the  $(i, j)^{th}$  entry of  $\mathbf{W}$  is of the form

$$\mathbf{W}_{ij} = \frac{\mathbf{T}_i^{11} * \mathbf{T}_j^{22} + \mathbf{T}_j^{11} * \mathbf{T}_i^{22} - \mathbf{T}_i^{12} * \mathbf{T}_j^{21} - \mathbf{T}_j^{12} * \mathbf{T}_i^{21}}{2} \quad (9)$$

Thus for a point  $\mathbf{x}$  lying on  $\mathbf{W}$  there exists a radial line,  $l'$  in the first radial image such that for any arbitrary  $l''$ , Eq. (5) is satisfied (or there exists a radial line in the second image such that for any arbitrary radial line in the first image, Eq. (5) is satisfied). Note that the above condition holds only for points  $\mathbf{x}$  which come from either line  $\mathbf{m}_1$ , which is the image of plane  $\Pi_1$  or  $\mathbf{m}_2$  which is the image of the plane  $\Pi_2$ . This implies that  $\mathbf{W}$  is a degenerate conic (pair of lines). Thus

$$\det(\mathbf{W}) = 0 \quad (10)$$

Eq. (10) is the degree-six internal constraint on the entries of  $\mathbf{T}_i^{jk}$ .

## 4. Computation of the Mixed Trifocal Tensor

The mixed trifocal tensor can be linearly estimated given atleast 11 corresponding triplets of features, with each triplet giving a linear constraint on the parameters of the tensor using Eq. (5). However this method would not impose the internal constraint we have discussed above. We will now describe a technique by which the degree-six internal constraint discussed above can be imposed.

Given 10 corresponding triplets of features, we obtain a  $10 \times 12$  measurement matrix and thus a two-dimensional right null-space. The trifocal tensor,  $\mathbf{T}$  can then expressed as

$$\mathbf{T} = \mathbf{Q} + \lambda \mathbf{R} \quad (11)$$

where  $\lambda$  needs to be determined.

Given two  $3 \times 2 \times 2$  tensors  $\mathbf{U}$  and  $\mathbf{V}$ , define an operator  $\mathbf{Y}(\mathbf{U}, \mathbf{V})$ , which gives as output a  $3 \times 3$  matrix, as following:

$$\mathbf{Y}_{ij} = \frac{\mathbf{U}_i^{11} * \mathbf{V}_j^{22} + \mathbf{V}_j^{11} * \mathbf{U}_i^{22} - \mathbf{U}_i^{12} * \mathbf{V}_j^{21} - \mathbf{V}_j^{12} * \mathbf{U}_i^{21}}{2} \quad (12)$$

The degree-six internal constraint expressed by Eq. (10) can be rewritten in the above terms (using Eq. (9) ) as:

$$\det(\mathbf{Y}(\mathbf{T}, \mathbf{T})) = 0 \quad (13)$$

Using Eq. (11), we can reduce Eq. (13) as following:

$$\begin{aligned} \det(\mathbf{Y}(\mathbf{T}, \mathbf{T})) &= 0 \\ \det(\mathbf{Y}(\mathbf{Q} + \lambda\mathbf{R}, \mathbf{Q} + \lambda\mathbf{R})) &= 0 \\ \det(\underbrace{\mathbf{Y}(\mathbf{Q}, \mathbf{Q})}_{\mathbf{D}_1} + \lambda(\underbrace{\mathbf{Y}(\mathbf{Q}, \mathbf{R}) + \mathbf{Y}(\mathbf{R}, \mathbf{Q})}_{\mathbf{D}_2}) + \lambda^2 \underbrace{\mathbf{Y}(\mathbf{R}, \mathbf{R})}_{\mathbf{D}_3}) &= 0 \end{aligned} \quad (14)$$

Note that in Eq. (14),  $\mathbf{D}_1$ ,  $\mathbf{D}_2$  and  $\mathbf{D}_3$  are known. Further, since the value of  $\lambda$  would be such that the determinant of  $\mathbf{D}$  is zero, there will exist  $\mathbf{z}$  such that:

$$(\mathbf{D}_1 + \lambda\mathbf{D}_2 + \lambda^2\mathbf{D}_3)\mathbf{z} = 0 \quad (15)$$

Computing the tuple  $(\lambda, \mathbf{z})$ , such that Eq. (15) is satisfied, is the standard Quadratic Eigenvalue Problem (QEP) [20] and can be efficiently solved. For example, in MATLAB, one can use the `polyeig` function.

Since the size of the minimal hypothesis is 10 and the kernel can be efficiently implemented ( $\mathbf{Q}$  and  $\mathbf{R}$  are estimated linearly and Eq. (15) can be solved efficiently), we can use a robust sieve, like RANSAC, to estimate the mixed trifocal tensor.

## 5. 3D Reconstruction

### 5.1. Projective Reconstruction

We now consider the problem of 3D reconstruction of points whose correspondences have been specified across the input images. Given the mixed trifocal tensor, we can easily compute the three uncalibrated camera matrices [8] . Once the projection matrices have been recovered, points in 3D can be reconstructed by back-projecting rays from the pin-hole camera and planes from the two radial cameras. If  $\mathbf{P} = [\mathbf{p}^1 \mathbf{p}^2 \mathbf{p}^3]^T$ ,  $\mathbf{P}' = [\mathbf{p}'^1 \mathbf{p}'^2]^T$ ,  $\mathbf{P}'' = [\mathbf{p}''^1 \mathbf{p}''^2]^T$  and  $\mathbf{x} = [x, y, z]^T$ ,  $\mathbf{l}' = [l'_1, l'_2]^T$ ,  $\mathbf{l}'' = [l''_1, l''_2]^T$  this corresponds to computing the right nullspace of the following matrix:

$$\begin{bmatrix} y\mathbf{p}^3 - z\mathbf{p}^2 \\ x\mathbf{p}^3 - z\mathbf{p}^1 \\ l'_2\mathbf{p}^1 - l'_1\mathbf{p}^2 \\ l''_2\mathbf{p}^1 - l''_1\mathbf{p}^2 \end{bmatrix} \quad (16)$$

Since only one plane and a ray are required to define a point uniquely in 3D space, we can infact reconstruct all points seen in the pin-hole camera and one of the radial views.

## 5.2. Metric Reconstruction

The dual absolute quadric,  $\Omega_\infty^*$  encodes both the absolute conic and the plane at infinity. To upgrade our reconstruction to metric, we need to estimate this degenerate quadric in the projective frame in which the cameras and the points have been determined [22, 15].  $\Omega_\infty^*$  projects into the radial 1D image as,

$$\tilde{\mathbf{K}}\tilde{\mathbf{K}}^T = \tilde{\omega}^* = \epsilon\mathbf{P}\Omega_\infty^*(\epsilon\mathbf{P})^T \quad (17)$$

with  $\tilde{\mathbf{K}} = \begin{bmatrix} f_x & s \\ 0 & f_y \end{bmatrix}$ ,  $\epsilon = \begin{bmatrix} 0 & 1 \\ -1 & 0 \end{bmatrix}$  the upper  $2 \times 2$  part of the calibration matrix. Using the assumptions of (i) *zero skew* ( $s = 0$ ) (ii) *known aspect ratio* ( $f_y = af_x$ ), we obtain 4 linear constraints on  $\Omega_\infty^*$ , from the 2 views. Under the assumptions of *zero skew*, *known aspect ratio*, *known principle point*, the pin-hole view yields 4 constraints on  $\Omega_\infty^*$  [9] to give a total of 8 constraints. Since  $\Omega_\infty^*$  is a  $4 \times 4$  homogeneous symmetric matrix it has 9 d.o.f (10 upto scale). Using the additional rank-3 constraint we obtain a fourth-degree equation ( $\det\Omega_\infty^* = 0$ ) and thus obtain upto 4 solutions. Only positive semi-definite solutions for the absolute quadric have to be considered. If  $\Omega_\infty^*$  is decomposed as  $\Omega_\infty^* = \tilde{\mathbf{H}}\tilde{\mathbf{I}}\tilde{\mathbf{H}}^T$  (where  $\tilde{\mathbf{I}} = \text{diag}(1, 1, 1, 0)$ ), then  $\mathbf{H}^{-1}$  is the point homography that takes the projective frame to the metric frame [9].

## 6. Special Case of Intersecting Optical Axes

We will now consider the special case when the optical axes of the two radial cameras intersect. This is interesting because we then would expect to have some close relationship with stereo (with the point of intersection of the two optical axes acting as the second camera center). Consider Figure 3. Once again let  $\mathbf{C}$  be the camera center and  $\mathbf{O}_1$  and  $\mathbf{O}_2$  be the two optical axes intersecting at  $\mathbf{C}_2$ . Let  $\mathbf{C}_2$  be imaged at  $\mathbf{x}$  in the first image. Note that any arbitrary choice of planes back-projected by the two radial cameras will intersect (at  $\mathbf{C}_2$ ) with the ray back-projected through  $\mathbf{x}$  by the pin-hole camera. An arbitrary choice of back-projected planes corresponds to an arbitrary choice of  $\mathbf{l}'$  and  $\mathbf{l}''$  in Eq. (5). Thus in this special case, *there always exists a  $\mathbf{x}$  (necessary condition) such that,*

$$\mathbf{T}_i^{jk} \mathbf{x}^i = 0 \quad \forall j \forall k \quad (18)$$

Eq. (18) implies that the matrix  $\mathbf{S}$  is rank-2 where,

$$\mathbf{S} = \begin{bmatrix} \mathbf{T}_1^{11} & \mathbf{T}_2^{11} & \mathbf{T}_3^{11} \\ \mathbf{T}_1^{12} & \mathbf{T}_2^{12} & \mathbf{T}_3^{12} \\ \mathbf{T}_1^{21} & \mathbf{T}_2^{21} & \mathbf{T}_3^{21} \\ \mathbf{T}_1^{22} & \mathbf{T}_2^{22} & \mathbf{T}_3^{22} \end{bmatrix} \quad (19)$$

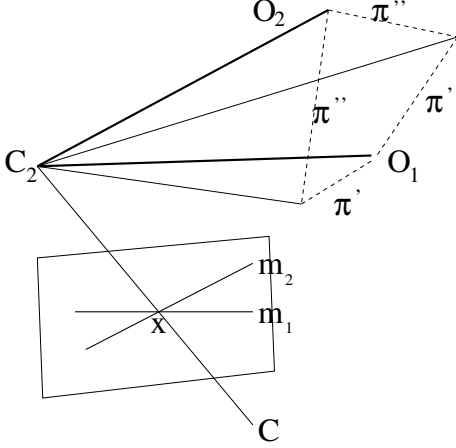


Figure 3:  $O_1$  and  $O_2$  are the two optical axes that intersect at  $C_2$ .  $C$  is the center of the pin-hole camera.  $O_i$  project onto  $m_i$ .  $C_2$  projects onto  $x$ , which is the intersection of  $m_1$  and  $m_2$ . Any arbitrary choice of planes  $\Pi'$  and  $\Pi''$  from the radial cameras, gives us a line that will pass through  $C_2$ . If we select  $x$  in the pin-hole image, any choice of planes from the radial images will intersect the ray back-projected from  $x$  (at  $C_2$ ).

We thus have the following condition,

$$\mathbf{T}_3^{jk} = \lambda \mathbf{T}_1^{jk} + \mu \mathbf{T}_2^{jk} \quad (20)$$

Using Eq. (9) we can prove that any  $\mathbf{T}$  that satisfies the condition in Eq. (20) also satisfies the internal constraint discussed in Eq. (10)<sup>2</sup>. It would then be a valid mixed trifocal tensor. It is then easy to prove that the Eq. (20) is also a *sufficient* condition for both the optical axes to intersect.

## 6.1. Estimation of $\mathbf{T}$

In this special case,  $\mathbf{T}$  has 9 degrees of freedom,  $8 - 1$  (for  $\mathbf{T}_1^{jk}$  and  $\mathbf{T}_2^{jk}$ ) + 2 (for  $\lambda, \mu$ ). We will now discuss a technique to estimate  $\mathbf{T}$  for this special case. Given 9 corresponding triplets of features, we have a  $9 \times 12$  measurement matrix and thus a 3-dimensional right null-space,

$$\mathbf{T} = \mathbf{L} + \gamma \mathbf{M} + \delta \mathbf{N} \quad (21)$$

where  $\gamma, \delta$  are scalars which need to be determined.

Given a  $3 \times 2 \times 2$  tensor,  $\mathbf{U}$ , define operators  $\mathbf{A}(\mathbf{U})$ ,  $\mathbf{B}(\mathbf{U})$  such that,

$$\mathbf{A}(\mathbf{U}) = \begin{bmatrix} \mathbf{U}_1^{11} & \mathbf{U}_2^{11} & \mathbf{U}_3^{11} \\ \mathbf{U}_1^{12} & \mathbf{U}_2^{12} & \mathbf{U}_3^{12} \\ \mathbf{U}_1^{21} & \mathbf{U}_2^{21} & \mathbf{U}_3^{21} \end{bmatrix} \quad \mathbf{B}(\mathbf{U}) = \begin{bmatrix} \mathbf{U}_1^{11} & \mathbf{U}_2^{11} & \mathbf{U}_3^{11} \\ \mathbf{U}_1^{12} & \mathbf{U}_2^{12} & \mathbf{U}_3^{12} \\ \mathbf{U}_1^{22} & \mathbf{U}_2^{22} & \mathbf{U}_3^{22} \end{bmatrix} \quad (22)$$

<sup>2</sup> $\mathbf{W}$  will be of the form  $\mathbf{W}_{3j} = \lambda \mathbf{W}_{1j} + \mu \mathbf{W}_{2j}$  and consequently be rank-2

Note that the condition expressed in Eq. (20) is equivalent to the following condition (both being the rank-2 condition):

$$\exists \mathbf{z}_1, \mathbf{z}_2 \quad s.t. \quad \mathbf{A}(\mathbf{T})\mathbf{z}_1 = 0 \quad and \quad \mathbf{B}(\mathbf{T})\mathbf{z}_2 = 0 \quad (23)$$

Substituting Eq. (21) in the above condition we obtain,

$$\begin{aligned} (\mathbf{A}(\mathbf{L}) + \gamma \mathbf{A}(\mathbf{M}) + \delta \mathbf{A}(\mathbf{N}))\mathbf{z}_1 &= 0 \\ (\mathbf{B}(\mathbf{L}) + \gamma \mathbf{B}(\mathbf{M}) + \delta \mathbf{B}(\mathbf{N}))\mathbf{z}_2 &= 0 \end{aligned} \quad (24)$$

where  $\gamma, \delta, \mathbf{z}_1$  and  $\mathbf{z}_2$  need to be determined.

Eq. (24) is the standard *Two-Parameter EigenValue Problem* [11]. Further, since all the matrices that are involved are  $3 \times 3$ , the solution technique would be extremely efficient.

Once again, considering the size of the minimal hypothesis (9 corresponding triplets) and the efficiency of implementation of the kernel ( $\mathbf{L}, \mathbf{M}, \mathbf{N}$  are estimated linearly and Eq. (24) can be solved efficiently), we can use a robust sieve like RANSAC for this special case also.

## 6.2. Relation to the Fundamental Matrix

One can compute the three projection matrices  $\mathbf{P}, \mathbf{P}'$  and  $\mathbf{P}''$ , given the trifocal tensor  $\mathbf{T}$ . Once again, let  $C$  be the center of the pin-hole camera and  $O_1$  and  $O_2$  be the two optical axes intersecting at  $C_2$ . Using the projection matrices, it is easy to compute, for the first radial camera, the radial line  $m'_1$  to which  $C$  projects and  $m'_2$  to which points on  $O_2$  project. Similarly we can compute the radial lines,  $m''_1$  and  $m''_2$ , in the second radial camera. Let  $\mathbf{G}$  be a coordinate transformation in the first radial image that takes  $m'_1$  to  $[0, 1]^T$  and  $m'_2$  to  $[1, 0]^T$ . Similarly let  $\mathbf{H}$  be the transformation in the second radial image. The trifocal tensor  $\mathbf{T}$  transforms as following:

$$\hat{\mathbf{T}}_i^{jk} = \mathbf{G}_s^j \mathbf{H}_t^k \mathbf{T}_i^{st} \quad (25)$$

If  $\hat{\mathbf{P}}, \hat{\mathbf{P}}'$  and  $\hat{\mathbf{P}}''$  correspond to the trifocal tensor  $\hat{\mathbf{T}}$ , it is easy to see that they will be of the form  $\hat{\mathbf{P}}' = [\hat{\Pi}^1 \hat{\Pi}^3]^T$ ,  $\hat{\mathbf{P}}'' = [\hat{\Pi}^2 \hat{\Pi}^3]^T$  (due to the choice of coordinates for  $m'_1, m'_2, m''_1, m''_2$  after the transformations  $\mathbf{G}$  and  $\mathbf{H}$ ), where  $\hat{\Pi}^1 = C \vee O_1$ ,  $\hat{\Pi}^2 = C \vee O_2$ ,  $\hat{\Pi}^3 = O_1 \vee O_2$ <sup>3</sup> (see Figure 4).

Let  $\hat{\mathbf{P}} = [\mathbf{p}^1 \mathbf{p}^2 \mathbf{p}^3]^T$  where  $\mathbf{p}^i$  denote the principal planes of the first pin-hole camera. Let us now examine the fundamental matrix,  $\mathbf{F}$  when the projection matrices are,  $\hat{\mathbf{P}}$  and  $\hat{\mathbf{P}} = [\hat{\Pi}^1 \hat{\Pi}^2 \hat{\Pi}^3]^T$ . Note that

$$\begin{aligned} \mathbf{F}_{r1} &= \eta_1 \det([\sim \mathbf{p}^r \quad \hat{\Pi}^2 \quad \hat{\Pi}^3]^T) \\ \mathbf{F}_{r2} &= \eta_2 \det([\sim \mathbf{p}^r \quad \hat{\Pi}^1 \quad \hat{\Pi}^3]^T) \\ \mathbf{F}_{r3} &= \eta_3 \det([\sim \mathbf{p}^r \quad \hat{\Pi}^1 \quad \hat{\Pi}^2]^T) \end{aligned} \quad (26)$$

<sup>3</sup>where  $\mathbf{A} \vee \mathbf{B}$  denotes the smallest subspace that contains  $\mathbf{A}$  and  $\mathbf{B}$ . In this case,  $\hat{\Pi}^i$  are planes.

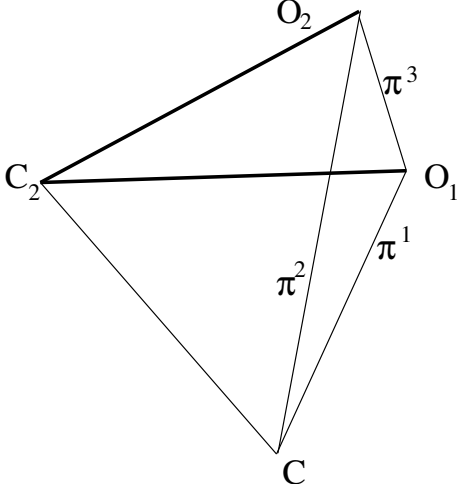


Figure 4: Relation to the Fundamental Matrix

where  $\eta_i = \pm 1$  and  $[\sim \mathbf{p}^r]$  is the matrix obtained from  $[\mathbf{p}^1 \mathbf{p}^2 \mathbf{p}^3]$  by omitting column  $\mathbf{p}^r$ .

Using the definition of the trifocal tensor,  $\hat{\mathbf{T}}$  in terms of the rows of the projection matrices,  $\hat{\mathbf{P}}$ ,  $\hat{\mathbf{P}}'$  and  $\hat{\mathbf{P}}''$  we have the following relation:

$$\begin{aligned} \mathbf{F}_{r1} &= \eta_1 \hat{\mathbf{T}}_r^{12} \\ \mathbf{F}_{r2} &= \eta_2 \hat{\mathbf{T}}_r^{21} \\ \mathbf{F}_{r3} &= \eta_3 \hat{\mathbf{T}}_r^{22} \end{aligned} \quad (27)$$

where  $\eta_i = \pm 1$ . Thus we see that the fundamental matrix of the cameras denoted by  $\hat{\mathbf{P}}$  and  $\tilde{\mathbf{P}}$  is embedded in the trifocal tensor  $\hat{\mathbf{T}}$  in this special case.

## 7. Conclusion

In this paper we have studied the mixed trifocal tensor that expresses the multi-view constraints among a pin-hole view and two 1D radial views. We have characterized the *only* internal constraint and given an efficient technique by which a solution can be obtained while enforcing it. We have given a method for computing a projective 3D reconstruction which can be upgraded to metric under the assumption of known internal parameters (with unknown focal length of the pin-hole camera). We have further studied the special case when the optical axes of the two radial 1D views meet at a point.

One obvious avenue of future work is validation of the above results on real and simulated data. Preliminary experiments are encouraging and show that the methods presented above are robust. We would also like to use the above methods while calibrating a hybrid camera network in the future.

## References

- [1] S. Baker and S. Nayar. A theory of single-viewpoint catadioptric image formation. *IJCV*, 35(2):1 – 22, 1999.
- [2] H. Bakstein and T. Pajdla. Panoramic mosaicing with a field of view lens. In *Proc. IEEE Workshop on Omnidirectional Vision*, pages 60–67, 2002.
- [3] Xilin Chen, Jie Yang, and Alex Waibel. Calibration of a hybrid camera network. In *ICCV*, pages 150–155, 2003.
- [4] F. Devernay and O.D. Faugeras. Straight lines have to be straight. *MVA*, 13(1):14–24, 2001.
- [5] C. Geyer and K. Daniilidis. Structure and motion from uncalibrated catadioptric views. In *CVPR*, volume 1, pages 279–286, 2001.
- [6] C. Geyer and K. Daniilidis. Paracatadioptric camera calibration. *PAMI*, 24(5):687–695, May 2002.
- [7] M. Grossberg and S. Nayar. A general imaging model and a method for finding its parameters. volume 2, pages 108–115, 2001.
- [8] R.I. Hartley and F. Schaffalitzky. Reconstruction from projections using grassmann tensors. In *ECCV*, pages Vol I: 363–375, 2004.
- [9] R.I. Hartley and A. Zisserman. *Multiple View Geometry in Computer Vision*. 2000.
- [10] R. Andrew Hicks and Ruzena Bajcsy. Catadioptric sensors that approximate wide-angle perspective projections. In *CVPR*, pages 545–551, 2000.
- [11] Michiel E. Hochstenbach, TomaKošir, and Bor Plestenjak. A Jacobi–Davidson type method for the two-parameter eigenvalue problem. Preprint 1262.
- [12] S.B. Kang. Catadioptric self-calibration. In *CVPR*, volume 1, pages 201–207, 2000.
- [13] J. Kannala and S. Brandt. A generic camera calibration method for fish-eye lenses. In *ICPR*, volume 1, pages 10–13, 2004.
- [14] B. Micusik and T. Pajdla. Estimation of omnidirectional camera model from epipolar geometry. In *CVPR*, pages I: 485–490, 2003.
- [15] M. Pollefeys, R. Koch, and L. Van Gool. Self-calibration and metric reconstruction in spite of varying and unknown internal camera parameters. volume 32, pages 7–25, 1999.

- [16] S. Shah and JK Aggarwal. Intrinsic parameter calibration procedure for a (high-distortion) fish-eye lens camera with distortion model and accuracy estimation. *Pattern Recognition*, 29(11):1175–1788, 1996.
- [17] P. Sturm and S. Ramalingam. A generic concept for camera calibration. In *ECCV*, volume 2, pages 1–13, 2004.
- [18] R. Swaminathan, M. Grossberg, and S. Nayar. Causatics of catadioptric camera. In *ICCV*, volume 2, pages 2–9, 2001.
- [19] R. Swaminathan and S.K. Nayar. Nonmetric calibration of wide-angle lenses and polycameras. *PAMI*, 22(10):1172–1178, October 2000.
- [20] Françoise Tisseur and Karl Meerbergen. The quadratic eigenvalue problem. Technical Report No. 370, Manchester, England, 2000.
- [21] B. Triggs. Matching constraints and the joint image. In *ICCV*, pages 338–343, 1995.
- [22] B. Triggs. Autocalibration and the absolute quadric. In *CVPR*, pages 609–614, 1997.
- [23] Reg Willson and Steven Shafer. What is the center of the image? In *CVPR*, pages 670 – 671, June 1993.
- [24] Y. Xiong and K. Turkowski. Creating image-based vr using a self-calibrating fisheye lens. In *CVPR*, pages 237–243, 1997.
- [25] X. Ying and Z. Hu. Catadioptric camera calibration using geometric invariants. In *ICCV*, 2003.